Bioinformatics analysis and identification of circular RNAs promoting the osteogenic differentiation of human bone marrow mesenchymal stem cells on titanium treated by surface mechanical attrition

Shanshan Zhu [1] , **Yuhe Zhu** [1] , **Zhenbo Wang** [2] , **Chen Liang** [2] , **Nan-Jue Cao** [3] , **Ming Yan** [1] , **Fei Gao** [4] , **Jie Liu** [Corresp., 5] , **Wei Wang** [Corresp. 1]

[1] School and Hospital of Stomatology, China Medical University, Liaoning Provincial Key Laboratory of Oral Diseases, Shenyang, Liaoning, China

[2] Shenyang National Laboratory for Materials Science,Institute of Metal Research, Chinese Academy of Sciences, Shenyang, Liaoning, China

[3] The Fourth Affiliated Hospital, Zhejiang University School of Medicine, Yiwu, Zhejiang, China

[4] School and Hospital of Stomatology, China Medical University, Liaoning Provincial Key Laboratory of Oral Diseases, Shenyang, China

[5] Department 1 of Science Experiment Center, China Medical University, Shenyang, Liaoning, China

Corresponding Authors: Jie Liu, Wei Wang
Email address: lj6152003@163.com, wwang75@cmu.edu.cn

Background. To analyse and identify the circular RNAs (circRNAs) involved in promoting the osteogenic differentiation of human bone mesenchymal stem cells (hBMSCs) on titanium by surface mechanical attrition treatment (SMAT).**Methods.** The experimental material was SMAT titanium and the control material was annealed titanium. Cell Counting Kits-8 (CCK-8) was used to detect the proliferation of hBMSCs, and alkaline phosphatase (ALP) activity and alizarin red staining were used to detect the osteogenic differentiation of hBMSCs on the sample surfaces.The bioinformatics prediction software miwalk3.0 was used to construct competing endogenous RNA (ceRNA) networks by predicting circRNAs with osteogenesis-related messenger RNAs (mRNAs) and microRNAs (miRNAs). The circRNAs located at the key positions in the networks were selected and analyzed by quantitative real-time PCR (QRT-PCR).**Results.** Compared with annealed titanium, SMAT titanium could promote the proliferation and osteogenic differentiation of hBMSCs. The total number of predicted circRNAs was 51. Among these, 30 circRNAs and 8 miRNAs constituted 6 ceRNA networks.Circ-LTBP2 was selected for verification. QRT-PCR results showed that the expression levels of hsa-circ-0032599, hsa-circ-0032600 and hsa-circ-0032601 were upregulated in the experimental group compared with those in the control group; the differential expression of hsa-circ-0032600 was the most obvious and statistically significant, with a fold change (FC) = 4.25 ± 1.60, p-values (p)< 0.05.

1 **Bioinformatics analysis and identification of circular RNAs**

2 **promoting the osteogenic differentiation of human bone**

3 **marrow mesenchymal stem cells on titanium treated by**

4 **surface mechanical attrition**

5 Shanshan Zhu[1,*], Yuhe Zhu[1,*], Zhenbo Wang[2], Chen Liang[2], Nanjue Cao[3], Ming Yan[1], Fei Gao[1], Jie Liu[4], Wei
6 Wang[1]

7 *[1] School and Hospital of Stomatology, China Medical University, Liaoning Provincial Key Laboratory of*
8 *Oral Diseases, Shenyang, Liaoning, China*

9 *[2] Shenyang National Laboratory for Materials Science,Institute of Metal Research, Chinese Academy of*
10 *Sciences, Shenyang, Liaoning, China*

11 *[3]The Fourth Affiliated Hospital, Zhejiang University School of Medicine, Yiwu, Zhejiang, China*

12 *[4]Department 1 of Science Experiment Center, China Medical University, Shenyang, Liaoning, China*

14 *[*]Authors contributed equally to this work*

15 *Corresponding Authors:*

16 *Wei Wang[1], Jie Liu[4]*

17 *[1] 117 Nanjing North Street, Heping District, Shenyang, Liaoning, 110002, China*

18 *Email address: wwang75@cmu.edu.cn*

19 *[4] 77 Puhe Road, Shenbei New District, Shenyang, Liaoning, 110013, China*

20 *Email address: lj6152003@163.com*

21   **Abstract**

22   **Background.** To analyse and identify the circular RNAs (circRNAs) involved in promoting the

23   osteogenic differentiation of human bone mesenchymal stem cells (hBMSCs) on titanium by

24   surface mechanical attrition treatment (SMAT).

25   **Methods.** The experimental material was SMAT titanium and the control material was annealed

26   titanium. Cell Counting Kits-8 (CCK-8) was used to detect the proliferation of hBMSCs, and

27   alkaline phosphatase (ALP) activity and alizarin red staining were used to detect the osteogenic

28   differentiation of hBMSCs on the sample surfaces. The bioinformatics prediction software

29   miwalk3.0 was used to construct competing endogenous RNA (ceRNA) networks by predicting

30   circRNAs with osteogenesis-related messenger RNAs (mRNAs) and microRNAs (miRNAs).

31   The circRNAs located at the key positions in the networks were selected and analyzed by

32   quantitative real-time PCR (QRT-PCR).

33   **Results.** Compared with annealed titanium, SMAT titanium could promote the proliferation and

34   osteogenic differentiation of hBMSCs. The total number of predicted circRNAs was 51. Among

35   these, 30 circRNAs and 8 miRNAs constituted 6 ceRNA networks. Circ-LTBP2 was selected for

36   verification. QRT-PCR results showed that the expression levels of hsa-circ-0032599, hsa-circ-

37   0032600 and hsa-circ-0032601 were upregulated in the experimental group compared with those

38   in the control group; the differential expression of hsa-circ-0032600 was the most obvious and

39   statistically significant, with a fold change (FC) = 4.25 ± 1.60, p-values (p)< 0.05.

40 **Conclusions.** Compared with annealed titanium, SMAT titanium can promote the osteogenic

41 differentiation of hBMSCs through circRNAs.

42 **Key words:** surface mechanical attrition treatment, human bone marrow mesenchymal ste

43 m cells, biological information prediction, circRNA, osteogenic differentiation

44

45 **Introduction**

46   Oral implant technology can effectively repair dentition defects. Compared with traditional

47 repair methods, oral implants have more beautiful shape, have stronger retention, result in higher

48 chewing efficiency and lower foreign body sensation, and can delay the absorption of alveolar

49 bone (Camargo WA et al., 2017). At present, dental implants are mainly made of pure titanium

50 and its alloys because titanium has a low density, low modulus, high strength, and excellent

51 biocompatibility and corrosion resistance (Song P et al., 2019; Duan M et al., 2019; Zhou W et

52 al., 2019). However, the corrosion resistance of titanium after implantation in the human body is

53 reduced, resulting in "stress shielding" that causes fibrous binding rather than osseointegration

54 and affecting the stability of the implants (Sven H et al., 2018; Ito T et al., 2018; Minko D,

55 Belyavin K, Sheleg V, 2017). Previous works showed that surface mechanical attrition treatment

56 (SMAT) technology might be applied to solve this problem by improving osseointegration

57 ability on Ti surface (Lai M et al., 2012). In addition, SMAT metals have the advantages of high

58 strength (T.H. Fang et al., 2011), decreased surface alloying temperature/time due to high

59 diffusion rate (Z.B. Wang, K. Lu, 2017) and high chemical reactivity (W.P. Tong et al., 2003),

60 and their wear resistance and fatigue resistance are also significantly improved (Z.B. Wang et al.,

61 2003; Y.B. Lei et al., 2019).

62   Human bone marrow mesenchymal stem cells (HBMSCs) are easy to acquire, isolate,

63 culture and purify. They have strong proliferation and differentiation potential. After many

64 passages, they still have the characteristics of stem cells; they function in haematopoietic support

65 and can secrete a variety of growth factors. They also have an immunoregulatory function and

66 show low immunological rejection characteristics (Son J W et al., 2018; Miranda H C et al.,

67 2012).

68   Circular RNA is double-stranded non-coding RNA that is bound by a covalent bond into a

69 closed loop structure without a 5' cap and 3' poly tail and is not easily degraded by exonucleases.

70 It is more stable than linear mRNA, and its length is between 200 bp and 2000 bp (Zhao R et al.,

71 2019; Ji H N et al., 2018); it is highly conserved, and it is found in eukaryotes, mostly within the

72 cytoplasm. A total of 16% of circRNAs are derived from coding genes, while 85% are derived

73 from exon rings. CircRNAs have specific reverse cleavage sites, and multiple circRNAs can be

74 produced at the same locus; this mainly occurs at the post-transcriptional level, and most

75 transcripts are non-encoding (Liu J et al., 2017; Zhao Z et al., 2018; Zhang M, Xin Y, 2018).

76 CircRNAs show specificity in terms of timing, organization, and disease specificity. They

77 accumulate in the nerve tissue during ageing and can be secreted from the outside of the cell to

78 form a ring in the membrane. The main types of circRNAs include exon circRNAs, exon-intron

79 circRNAs, intron circRNAs, antisense circRNAs, intergenic circRNAs, and sensory-overlap

80 circRNAs. The main functions of circRNAs are as follows: to function as ceRNA molecules (as

81 miRNA molecular "sponges") to bind to miRNA response elements (MREs) to reduce the effects

82 of miRNA on gene expression; to regulate classical RNA splicing so that classical RNA is

83 inhibited; to regulate parental gene transcription (Kulcheski F R, Christoff A P, Margis R., 2016;

84 Cortéslópez M et al., 2018); to bind to RNA-binding proteins to regulate other RNAs; to be

85 translated into proteins; to induce pseudogene expression after reverse transcription (Li S, Han L,

86 2019).

87   A large number of studies in recent years have shown that circRNA can regulate stem cell

88 osteogenic differentiation. Zhang et al. (Mengjun Z, Lingfei J, Yunfei Z, 2018) performed

89 microarray analysis to determine the expression profile of circRNAs during osteoblast

90 differentiation. The results indicated that the functional annotation of differentially expressed

91 circRNAs was associated with osteogenic differentiation. The researchers then constructed a

92   circRNA-miRNA network, and network analysis indicated that some circRNAs were associated

93   with miRNAs with osteogenic effects. In addition, the researchers verified the expression of a

94   central miRNA, miR-199b-5p, and its associated circ RNA circIGSF11. The results showed that

95   silencing circIGSF11 can promote osteoblast differentiation; Zheng et al. (Zheng Y et al., 2017)

96   induced periodontal ligament stem cells (PDLSCs), which were analysed by circRNA

97   sequencing, qRT-PCR, differential expression analysis and gene ontology (GO) analysis. The

98   target mRNAs regulated by the differentially expressed circRNAs were enriched in cell matrix

99   formation and osteogenic differentiation.

100   This study intends to use biological information prediction to analyse the interactions

101   between miRNAs, circRNAs, and circRNA-miRNA-mRNA that interact with osteogenic

102   mRNAs. It also seeks to investigate whether the SMAT titanium material can promote hBMSC

103   osteogenic differentiation by affecting circRNA and provide a theoretical basis for the

104   application of SMAT in oral clinic.

105

106   **Materials & Methods**

107   1. Preparation of titanium sheets

108   Experimental group: Pure titanium plates in medical grade, in a cylindrical shape with a

109   diameter of 60 mm and a thickness of 5 mm, were studied in this work. We performed

110   ultrasonic-assisted SMAT on the plate samples by using a SNC-2 machine (New Nano-crystal

111   Technology Co., Ltd., China) at a frequency of 20000 Hz. During SMAT,   hardened steel balls

112   with a diameter of 6 mm were driven by the system and repeatedly impacted onto the sample

113   surface for 30 min, so that a gradient nanostructured surface layer was formed. The SMAT plates

114   were electrically spark-cut into discs with a diameter of 11 mm and a thicknesses of 2.5 mm, as

115   the samples in the experimental group.

116   Controlled group: An annealing treatment was carried out at 680 °C for 2 hours on the

117   SMAT samples to prepare the samples in the controlled group. By doing this, the surface

118   morphologies of the experimental and controlled samples were similar, while the grains in the

119   surface layer of the controlled samples became coarse.

120   Samples in both the experimental and controlled groups were sequentially cleaned in

121   acetone, 36%-38% dilute hydrochloric acid, absolute ethanol and distilled water, and then

122   ultrasonically washed for 20 minutes, dried and autoclaved prior to use.

123   Transmission electron microscope (TEM; JEOL, Japan) was used to observe the surface

124   structure of the experimental materials so as to determine whether it has gradient nanostructures.

125   2. Culture of hBMSCs

126   HBMSCs were purchased from Beijing Yuhengfeng Technology Co., Ltd. We resuscitated

127   the 10th generation of hBMSCs and placed them in α-modified Eagle medium (αMEM, HyClone)

128   containing 15% foetal bovine serum (FBS, HyClone) and 100 U/ml double antibody (HyClone),

129   and the cells were cultured at 37 °C in a 5% CO_2 cell culture incubator. The cells were in the

130   logarithmic phase of growth during all experiments.

131   3. CCK-8 method for determining the cell proliferation curve

132   The 14th generation hBMSCs showing good growth were inoculated at $4 \times 10^4/cm^2$ on

133   SMAT titanium and annealed titanium, which were placed in 24-well plates. Each group of

134   materials was placed in 3 wells. Each well was filled with 1 ml of basic medium. A total of 100

135   μl of CCK-8 (KGI Biotechnology Co., Ltd., China) was added to each well on day 1, 3, 5, and 7.

136   We incubated the plates for 2 hours at 37 °C. Then, we pipetted 110 μl of reaction solution per

137   well into a 96-well plate. A microplate reader (Tecan, Switzerland) was used to detect the optical

138   density (OD) value of each well at a wavelength of 450 nm. The proliferation curve of the 14th

139   generation of hBMSCs was generated with time as the horizontal axis and the average OD as the

140   vertical axis.

141   4. ALP activity detection

142   We inoculated 14th generation hBMSCs showing good growth at $4\times10^4/cm^2$ on SMAT

143   titanium and annealed titanium, which were placed in 24-well plates. Each group of materials

144   was placed in 3 wells, and each well was supplemented with 1 ml basic culture solution. When

145   the cell fusion degree was 80%-90%, we added osteogenic induction medium(15% FBS, 1%

146   streptomycin mixture, 10^{-7}M dexamethasone,10^{-2} β-glycerophosphate disodium salt, 50μg/ml

147   Vitamin C, αMEM)and cultured the cells in a 37 °C incubator. After 3, 5, 7, and 14 days of

148   culture, we digested the cells of each group with trypsin (Solarbio). We lysed the cells with 1%

149   Triton X-100 (Solarbio) and repeatedly thawed them until they were disrupted, and then we

150   collected the supernatant. The ALP activity of each group of cells was determined and calculated

151   according to the instructions in the ALP activity test kit (Institute of Bioengineering, Nanjing,

152   China) and Bradfords (BCA) kit (Institute of Bioengineering, Nanjing, China).

153   5. Alizarin red staining

154   The 14th generation hBMSCs showing good growth were inoculated at $4\times10^4/cm^2$ on

155   SMAT titanium and annealed titanium, which were placed in 24-well plates. Each group of

156   materials was plated in 3 wells supplemented with 1 ml basic culture solution. When the cell

157   fusion degree was 80%-90%, we added osteogenic induction medium and cultured the cells in a

158   constant temperature incubator. After 7, 14, and 21 days of culture, we fixed the cells in 95%

159   ethanol for 1 hour and stained them with 1% Alizarin red (Sigma) for 2 hours.

160   6. Biological information prediction

161   (1) Prediction and screening of osteogenesis-related miRNAs

162   The osteogenesis-related literature from 2015 to 2019 was used to select 20 osteogenesis-

163   associated mRNAs. Twelve mRNAs associated with the transforming growth factor-β (TGF-β)/

164   drosophila mothers against decapentaplegic protein (Smad), mitogen-activated protein kinase

165   (MAPK)/ extracellular signal-regulated kinase (ERK), Wnt, and Notch signalling pathways were

166 analysed and screened in combination with Kyoto Encyclopaedia of Genes and Genomes

167 (KEGG) signalling pathway analysis. MiRNAs 3.0 software was used to screen for miRNAs

168 capable of targeting these candidate mRNAs. The underlying screening principle involved the

169 identification of miRNAs that were located in the seed area as predicted by TargetScan, miRDB

170 and miwalk3.0.

171 (2) The prediction and screening of osteogenesis-related circRNAs

172 The formation of circRNA is based on exon cyclization. Miwalk3.0 software was used to

173 screen the complementary sequence of the coding sequence (CDS) region of the obtained

174 miRNA, and the mRNA sequence of the seed region was used as the source transcript for the

175 circRNA. The exon of each gene was searched based on the complementary region, and the

176 circRNA including the exon was screened. The length of the circRNAs selected for the

177 experiment were 200-2000 bp, and each was detected in more than 2 samples from the circBase.

178 (3) Predictive analysis of ceRNA networks of osteogenesis-related circRNAs

179 The mRNA-miRNA-circRNA interactions were analysed to determine the frequency

180 distribution, and network analysis was performed by using Cytoscape software to identify the

181 core molecules and construct the ceRNA networks. The interactions between them were

182 analysed, and the selected circRNAs located at key locations in the networks were used for qRT-

183 PCR verification.

184 7. QRT-PCR detection of the differential expression of circRNAs during the osteogenic

185 differentiation of hBMSCs on the two groups of titanium plates

186 The 14th generation hBMSCs showing good growth were inoculated at $4 \times 10^5 / cm^2$ on

187 SMAT titanium and annealed titanium in 6-well plates. We used 3 wells for each set of materials,

188 and each well was filled with 3 ml of basic culture solution. When the cell fusion degree was

189 80%-90%, we added osteogenic induction medium and cultured the cells in a constant

190 temperature incubator. Once the cells had been osteogenically induced for 3, 5, 14, 21 days, two

191   sets of total RNA were separately extracted with TRIzol (Gibco), and the purity and amount of

192   the collected RNA were determined by a Nanodrop 2000 microultraviolet analyser (Thermo

193   Company, USA). CDNA was synthesized using the PrimeScript RT Master Mix (Takara, Japan).

194   Shengong Biological Engineering Co., Ltd. (Shanghai, China) designed specific primers for the

195   circRNAs. QRT-PCR was performed using TB Green Premix EX TaqTM II (Takara, Japan), and

196   PCR-specific amplification was conducted with a Prism 7500 real-time PCR instrument (ABI

197   Company, USA). The expression of circRNAs was determined based on the threshold cycle (Ct),

198   and the relative expression levels were calculated using the $2^{-\Delta\Delta Ct}$ method. GAPDH served as an

199   internal standard control. The primer and internal reference fragment sequences (5'-3') are as

200   Table 1.

201   8. Statistical analysis

202   All experiments were repeated three times. SPSS Statistics 20.0 software and GraphPad

203   Prism 7 were used to perform the statistical analyses. We used one-way ANOVA and the LSD-t

204   test to compare data between groups. Data are expressed as the mean ± standard deviation, and

205   the differences with a FC≥ 2.0 and a $p<$ 0.05 were considered statistically significant.

206

207   **Results**

208   1. Preparation of titanium

209   The TEM observation shows that the SMAT method can make the surface of gradient nano-

210   metal pure titanium nanocrystallization, and the grain size is on the nanometer scale (Fig. 1).

211   2. Culture of hBMSCs

212   HBMSCs were observed as adherent cells under an inverted phase contrast microscope.

213   One day after passage, the cells were partially attached (Fig. 2A); after 3 days, most of the cells

214   were adherent, and the cell fusion degree was over 80%. The morphology of the adherent cells

215 changed from round to long fusiform or star-shaped, and the arrangement was spiral (Fig. 2B).

216 3. Proliferation curve of the hBMSCs

217 (1) After observing the hBMSC subculture for 7 days, the results showed that the hBMSCs

218 showed obvious latency, logarithmic proliferative and plateau phases, and the growth curve

219 assumed an "S" shape. Days 1-3 were the incubation period, and days 3-5 were the logarithmic

220 growth phase; On the 3rd and 5th day of culture, the difference between the SMAT titanium

221 group and the annealed titanium group was statistically significant ($p < 0.05$; Fig. 2C).

222 4. Detection of ALP activity

223 When hBMSCs were cultured for 3, 5, 7 and 14 days, the ALP activity level in each group

224 increased over time. At each time point, the level of ALP activity in the SMAT titanium group

225 was higher than that in the annealed titanium group. On days 3 and 5, the differences between

226 the SMAT titanium group and the annealed titanium group were statistically significant ($p < 0.05$;

227 Fig. 3D). It is shown that SMAT titanium can promote the early osteogenic differentiation of

228 hBMSCs.

229 5. Alizarin red staining

230 HBMSCs were induced osteogenically for 7, 14 and 21 days, and the alizarin red staining

231 area of each group increased over time. At each time point, the alizarin red staining area of the

232 SMAT titanium group was larger than that of the annealed titanium group. On the 14th day, the

233 difference between the SMAT titanium group and the annealed titanium group was statistically

234 significant ($p < 0.05$; Fig. 3ABC and Fig. 3E). It is shown that SMAT titanium can promote the

235 late osteogenic differentiation of hBMSCs.

236 6. Biological information prediction

237 (1) Screening results for the osteogenesis-related miRNAs

238 According to the literature, 20 osteogenesis-related mRNAs have been identified, including

239 ALK, COLIA1, RUNX2, SP7, IBSP, COL10VA1, BMP2, BGLAP, SPP1, DLX5, CBFB, BMP7,

240 AcvR1b, LIF, INHBA, Noda1, BMP4, FGF2, IGF1, Wnt. Twelve mRNAs were confirmed to be

241 involved in the TGF-β/ Smad, MAPK/ ERK, Wnt, and Notch signalling pathways, including

242 Wnt3, Wnt4, Wnt8B, RUNX2, IGF1, ACVR1B, INHBC, CBFB, LIF, BMP7, NOG, CHRD.

243 Among them, Wnt3, Wnt4 and Wnt8B genes are involved in the Wnt signalling pathway, the

244 RUNX2 gene is involved in the Notch signalling pathway, the CBFB gene is involved in the

245 Smad2/3 signalling pathway, the LIF gene is involved in the ERK signalling pathway, the IGF1

246 is involved in the MAPK/ ERK signalling pathway, the INHBC, ACVR1B, NOG, CHRD genes

247 are involved in the TGF-β signalling pathway, and the BMP7 gene is involved in the TGF-β and

248 ERK signalling pathways (Fig. 4C-L).

249   Eight miRNAs were predicted, including hsa-miR-18b-5p, hsa-let-7b-5p, hsa-miR-1224-5p,

250 hsa-miR-129-5p, hsa-miR-145-5p, hsa-miR-24-3p, hsa-miR-5195-3p, hsa-miR-6088 (Table 2).

251 (2) Screening results for the osteogenesis-related circRNAs

252   Fifty-one circRNAs were screened by miwalk3.0 software (Table 3, Fig. 4AB).

253 (3) CeRNA network analysis of the osteogenesis-related circRNAs

254   Further analysis of the predicted 51 circRNAs revealed that 30 circRNAs and 8 miRNAs

255 constituted 6 ceRNA networks. Circ-GNB5/ circ-HERC1/ circ-KMT2A/ circ-LTBP2 interact

256 with hsa-miR-24-3p and Wnt3 gene in the Wnt signaling pathway; circ-TBC1D2B/ circ-TBCD/

257 circ-TRIOBP/ circ-VPS13C interact with hsa-miR-6088 and CBFB gene in the Smad2/3

258 signaling pathway; circ-ABCA3 interacts with hsa-miR-18b-5p and CF2L2;circ-MDN1/ circ-

259 MYH9/ circ-PLPPR4/ circ-RAB31/ circ-SMARCH2/ circ-SPEG/ circ-SYNM/ circ-TANGO6

260 interact with hsa-miR-5195-3p and Wnt4 gene in the Wnt signaling pathway, the IGF1 gene in

261 the MAPK/ERK signaling pathway; hsa-miR-1224-5p combines with NOG gene in the TGF-β

262 signaling pathway; circ-ADAMTS13/ circ-ARHGAP32/ circ-BRPF3/ circ-CARD8/ circ-

263 CCDC88C/ circ-COL4A2/ circ-DGKD/ circ-DIP2C/ circ-DYNC1H1/ circ-FAT3/ circ-LTBP2

264   interact with hsa-let-7b-5p and CHRD gene in the TGF-β signaling pathway (Fig 4M).

265   7. QRT-PCR assay

266   To verify the accuracy of the bioinformatics prediction, we screened circ-LTBP2 expression

267   by using QRT-PCR detection. The results of QRT-PCR showed that the expression levels of hsa-

268   circ-0032599, hsa-circ-0032600 and hsa-circ-0032601 were upregulated in the experimental

269   group, and the differential expression of hsa-circ-0032600 was the most upregulated and

270   statistically significant on the 14th day (FC= 4.25±1.60, $p< 0.05$; Fig. 5).

271

272   **Discussion**

273   SMAT technology uses high-energy balls to repeatedly impact the sample surface.

274   Typically, a gradient nanostructured surface layer, in which the grain size is in the nanometer

275   scale at the top surface and gradually increases into the micrometer scale in the interior, will be

276   achieved on metals by SMAT (T.H. Fang et al., 2011; Lu K, Lu J, 2004). In this study, the TEM

277   observation shows that the SMAT method can make the surface of gradient nano-metal pure

278   titanium nanocrystallization, and the grain size is on the nanometer scale. Since there is no

279   interface separating the surface layer and the substrate, the problem of poor interface bonding

280   between the nanostructured surface layer and the substrate, usually caused by traditional coating

281   techniques, is easily solved (Nana L, Ning W, 2018; Du H et al., 2019). In addition, SMAT

282   materials have the advantages of high strength, high hardness, high diffusion rate and high

283   chemical reactivity, and their wear resistance and fatigue resistance are also significantly

284   improved (Nowak W J, Serafin D, Wierzba B, 2019; Benafia S et al., 2018; Yao Q et al., 2017;

285   T.H. Fang et al., 2011; Z.B. Wang, K. Lu, 2017; W.P. Tong et al., 2003; Z.B. Wang et al., 2003;

286   Y.B. Lei et al., 2019; Lu K, Lu J, 2004). In this study, the influence of surface morphologies on

287   the adhesion, proliferation and differentiation of hBMSCs might be safely excluded, while the

288   samples in the experimental and controlled groups show a similar surface morphology (with

289   surface roughness R_a of 1.73±0.11 and 1.82±0.06 μm, respectively). Therefore, it should be the

290   contribution from the surface nanostructure that the hBMSC osteogenic differentiation is

291   promoted on the SMAT titanium.

292   In this study, hBMSCs can differentiate into osteoblasts. A lot of literature have confirmed

293   that hBMSCs are important members of a family of stem cells and are derived from early

294   developing mesoderm and ectoderm. They are easy to extract and purify, and they still show

295   stem cell characteristics after repeated subculturing. They have strong proliferation and

296   differentiation ability and can be multi-directionally differentiated into osteoblasts, chondrocytes,

297   haematopoietic cells, muscle cells and other types of cells. They can be used to repair tissue and

298   organ damage (Saito A et al., 2018; Mohammadali F, Abroun S, Atashi A, 2018). They have a

299   haematopoietic support function, since they not only provide mechanical support for

300   haematopoietic stem cells in the bone marrow but also secrete a variety of growth factors, such

301   as interleukin (IL)-6, IL-11, leukaemia inhibitory actor (LIF), macrophage colony-stimulating

302   factor (M-CSF) and human stem cell growth factor (SCF), to support haematopoiesis (Amini A

303   et al., 2018; Mohammadali F, Abroun S, Atashi A, 2018). HBMSCs also regulate immune

304   function and do not show immunological characteristics consistent with rejection (Liu C et al.,

305   2018; Gabr M M et al., 2017; Lee H J et al., 2017).

306   To date, several osteogenesis-related signalling pathways have been documented, including

307   the TGF-β, Smad, MAPK, Wnt/ β-catenin, Notch, Hedgehog, fibroblast growth factor (FGF),

308   and orthopantomography (OPG)/ receptor activator for nuclear factor-κB ligand (RANKL)

309   signalling pathways (Zhu W Q et al., 2018; Urbanek K et al., 2017; Jin L et al., 2017). TGF-β

310   can increase intracellular ALP activity and the synthesis and secretion of osteocalcin, collagen,

311   and osteonectin (Yang S et al., 2018). The TGF- β pathway consists of extracellular ligands,

312   transmembrane receptors, and intracellular regulatory factors. The receptor TGF-β activates

313   Smads and enters the nucleus, thereby regulating its target genes (Hui L et al., 2018); the MAPK

314   signalling pathway involves MAPK/ ERK/ big MAP kinase 1 (BMK1)/ stress activated protein

315   (SAPK)/ c-Jun N-terminal kinase (JNK)/ P38 in five main ways (Lou R et al., 2019; Jiang L et al.

316   2018). The MAPK signalling pathway also plays an important role in the proliferation,

317   differentiation and apoptosis of osteoblasts (Li Z H et al., 2018). Wnt signalling plays an

318   important role in the proliferation and differentiation of mesenchymal stem cells,

319   osteoblastogenesis, bone formation, bone remodelling, and other processes (Wang X et al., 2019;

320   Shuai Y et al., 2019). The Wnt signalling pathway can also be involved in cell-to-cell signalling

321   through paracrine or autocrine signalling and participates in a variety of cellular processes, such

322   as cell proliferation, differentiation, polarization, and migration (Hang K et al., 2019; Jun-Li Liu

323   et al., 2017). The Notch signalling pathway involves the Notch receptor, DSL protein (ligand),

324   DNA binding protein and Notch regulatory molecule. It can play a role in multiple cell

325   morphogenetic processes, such as cell formation, differentiation, and apoptosis (Nandagopal N et

326   al., 2018; Sun Z et al., 2018; Carra S et al.,2017). In this study, we choose twelve osteogenesis-

327   related mRNAs associated with the TGF-β/ Smad, MAPK/ ERK, Wnt, and Notch signalling

328   pathways to predict osteogenesis-related miRNAs and circRNAs.

329   This study proves that there are differences in the expressions of osteogenesis-related

330   circRNAs in the process of SMAT titanium promoting the osteogenic differentiation of hBMSCs.

331   Currently, a large number of studies have shown that circRNA can regulate stem cell osteogenic

332   differentiation. Gu et al. cultured PDLSCs in osteogenic induction medium and normal medium

333   and found differences in the expression of a total of 1456 circRNAs by RNA sequencing. The

334   researchers used GO and KEGG analyses to predict that circRNA-BANP and circRNA-ITCH

335   can regulate the osteogenic differentiation of PDLSCs through the MAPK pathway (Gu X et al.,

336   2017). Li et al. (Xiaobei L et al., 2018) used qRT-PCR to detect the expression level of CDR1as

337   during the osteogenic differentiation of PDLSCs and constructed CDR1as overexpression and

338   silencing models to detect osteogenic differentiation. Animal experiments were performed to

339   analyse the formation of new bone by microcomputed tomography and various staining methods.

340   The results showed that CDR1as was upregulated and that silencing CDR1as could inhibit the

341   osteogenic differentiation of cells. In vivo experiments have shown that silencing CDR1as can

342   inhibit bone formation.

343   Alkaline phosphatase is a sugar protease released by cytoplasmic special particles. It

344   hydrolyzes phosphate esters during osteogenesis, provides phosphoric acid for hydroxyapatite

345   deposition, and hydrolyzes pyrophosphate to relieve its inhibitory effect on bone salt formation.

346   Its activity level is positively correlated with the degree of osteogenic differentiation of cells. It is

347   an early marker of osteogenic differentiation of hBMSCs (Samuel S et al., 2016; Li R et al.,

348   2019). The sample was reacted in a carbonate buffer (pH = 9.8) containing p-nitrobenzene

349   phosphate. Under the action of alkaline phosphatase in the sample, p-nitrobenzene phosphate

350   was decomposed into p-nitrophenol and phosphoric acid. The resulting p-nitrophenol is basic

351   and yellow. Based on measuring the absorbance at 405 nm, the alkaline phosphatase activity in

352   the sample was calculated. The hBMSCs on each group of materials gradually increased ALP

353   activity after osteogenesis induction, and the ALP activity of the SMAT group was higher than

354   that of the annealed group at each time point. On the 3rd and 5th days, the difference between the

355   SMAT group and the annealed group was statistically significant ($p<0.05$). It is shown that

356   nanostructure can promote the early osteogenic differentiation of hBMSCs. Alizarin red is an

357   anionic dye that forms a red complex with metal ions. It can recognize and chelate calcium ions

358   to form orange-red calcium nodules. It is a sign of late osteogenic differentiation (Li R et al.,

359   2019). The area of alizarin red staining of cells on both groups of materials gradually increased

360   with the increase of culture time. At each time point of detection, the alizarin red staining area of

361   the SMAT group was larger than that of the annealed group. This shows that SMAT titanium has

362   better ability to promote the osteogenic differentiation of hBMSCs in late stage than annealed

363   titanium. On the 14th day, the difference between the SMAT group and the annealed group was

364   statistically significant ($p<0.05$). It is shown that nanostructures can promote the late osteogenic

365   differentiation of hBMSCs.

366   In the predicted ceRNA networks, one combination of circ-GNB5, circ-HERC1, circ-

367   KMT2A, circ-LTBP2, hsa-miR-24-3p and the Wnt3 gene, another comprised of circ-LTBP2,

368   circ-MCF2L2, circ-MDN1, circ-MYH9, circ-PLPPR4, circ-RAB31, circ-SMARCH2, circ-SPEG,

369   circ-SYNM, circ-TANGO6, hsa-miR-5195-3p and the Wnt4, IGF1 genes, the third consist of

370   circ-ADAMTS13, circ-ARHGAP32, circ-BRPF3, circ-CARD8, circ-CCDC88C, circ-COL4A2,

371   circ-DGKD, circ-DIP2C, circ-DYNC1H1, circ-FAT3, circ-LTBP2, hsa-let-7b-5p and CHRD,

372   three networks communicated with each other through the core hub circ-LTBP2. Based on the

373   previous prediction, it's target mRNAs including wnt3, wnt4, CBFB, IGF1 and CHRD are

374   recognized osteogenic marker genes (Kureel J et al., 2017; Qin X et al., 2015; Lindsey R C et al.,

375   2018). What's more, circ-LTBP2 has not been reported yet. So we selected circ-LTBP2 for

376   verification.

377   In the comparison of the two groups of materials, QRT-PCR results showed that the

378   differential expression of hsa-circ-0032600 on the 14th day was significant (p-values), which is

379   consistent with the results of alizarin red staining. The combination mRNAs of hsa-circ-0032600

380   including wnt3, wnt4, CBFB, IGF1, CHRD involved in Wnt, Smad2/3, MAPK / ERK, TGF-β

381   osteogenic pathways, which can regulate osteogenic differentiation in the middle and late stages

382   (Mobini S et al., 2017; Li R et al., 2019; Mao X Y et al., 2012). So hsa-circ-0032600 can

383   regulate the osteogenic differentiation of hBMSCs n the middle and late stages. However, vivo

384   experiments are still needed to confirm that hsa-circ-0032600 in promoting osteogenic

385   differentiation. And whether it can act as ceRNA, that is, the molecular sponge of miRNA, so as

386   to reduce the effect of miRNA on gene expression still needs to be further investigated.

387

388   **Conclusions**

389   In this paper, we predict that the role of circ-LTBP2, which is shared by hsa-miR-24-3p,

390   hsa-let-7b-5p and hsa-miR-5195-3p in osteogenic differentiation, still needs further experimental

391   investigation. By using the prediction of the circRNAs that interact with 12 mRNAs and 8

392   miRNAs related to osteogenesis, it is necessary to further explore whether the relevant circRNA-

393   miRNA-mRNA interactions function as sponges during osteogenic differentiation.

394   In summary, our research firstly first involved biological information prediction. According

395 to the KEGG analysis of circRNA parent genes, we identified 30 circRNAs and 8 miRNAs that

396 form 6 ceRNA networks. Moreover, the circRNAs located in key positions in the networks were

397 identified as being involved in the potential ceRNA mechanism of the circRNA-miRNA-mRNA

398 network, and their expression differences were verified by QRT-PCR analysis. To the best of our

399 knowledge, the role of hsa-circ-0032600 that was verified in this study has not yet been reported.

400 Therefore, this study demonstrates that SMAT titanium material can promote hBMSC osteogenic

401 differentiation by affecting circRNAs, and this material can be used clinically.

402

403 **ACKNOWLEDGEMENTS**

404 We thank Mingshan Li for guiding us about the bioinformatics.

405 **ADDITIONAL INFORMATION AND DECLARATIONS**

406 **Funding**

407 This study was supported by National Natural Science Foundation of China (No. 81970980),

408 Liaoning Provincial Key Research Plan Guidance Project (No. 2018225078), Liaoning

409 Provincial Natural Science Foundation Guidance Project (NO. 2019-ZD-0749) and Shenyang

410 Major Scientific and Technological Innovation Research and Development Plan (NO. 19-112-4-

411 027), Shenyang National Laboratory for Materials Science (No. 2015RP04). The funders had no

412 role in study design, data collection and analysis, decision to publish, or preparation of the

413 manuscript.

414 **Grant Disclosures**

415 The authors declare that they have no grant disclosures.

416 **Competing Interests**

417 The authors declare that they have no competing interests.

418 **Author Contributions**

419 Wei Wang conceived and designed the experiments, and helped improve this paper.

420 Shanshan Zhu and Yuhe Zhu collected the samples, performed the experiments, analyzed the
421 data, prepared the figures and tables, and wrote this paper.

422 Jie Liu contributed the equipments and analysis tools, and revised this paper critically for
423 important content.

424 Zhenbo Wang participated in designing experimental routes and writing the manuscript
425 (preparation and microstructure of Ti samples).

426 Chen Liang helped prepare the SMAT and annealed Ti samples.

427 Nanjue Cao, Mingyan and Feigao helped improve the figures.

428

429 **References**

430 1. Camargo WA, Takemoto S, Hoekstra JW, Leeuwenburgh SC.G, Jansen JA, Beucken
431 JJ.J.P.vd, Alghamdic HS. 2017. Effect of surface alkali-based treatment of titanium implants
432 on ability to promote in vitro mineralization and in vivo bone formation. ACTA
433 BIOMATERIALIA 57:511 DOI:10.1016/j.actbio.2017.05.016.

434 2. Song P, Hu C, Pei X, Sun J, Sun H, Wu L, Jiang Q, Fan H, Yang B, Zhou C, Fan Y,
435 Zhang X. 2019. Dual modulation on crystallinity and macro/micro structures of 3D printed
436 porous titanium implants to enhance the stability and osseointegration. Journal of Materials
437 Chemistry B 7 DOI:10.1039/C9TB00093C.

438 3. Duan M, Wu X, Yuan L, Zhang Z, Zhang Y, Zhou Y. 2019. Fabrication and In vitro
439 Bioactivity of Robust Hydroxyapatite Coating on Porous Titanium Implant. Chemical
440 Research in Chinese Universities 35: 686-692 DOI:10.1007/s40242-019-9101-x.

441   4. Zhou W, Huang O, Gan Y, Li Q, Zhou T, Xi W. 2019. Effect of titanium implants

442   with coatings of different pore sizes on adhesion and osteogenic differentiation of BMSCs.
443   Artificial Cells, Nanomedicine, and Biotechnology 47:290-299.

444   5. Sven H, Christoph A, Tarek E, Deml M, Milavec H, Bigdon SF, Benneker LM. 2018.

445   First Results of a New Vacuum Plasma Sprayed (VPS) Titanium-Coated Carbon/PEEK
446   Composite Cage for Lumbar Interbody Fusion. Journal of Functional Biomaterials 9:23
447   DOI:10.3390/jfb9010023.

448   6. Ito T, Ohtsu N, Tomozawa M, Takita H, Iizuka T, Yokoyama A. 2018. Promotion of

449   bone regeneration on titanium implants through a chemical treatment process using calcium
450   phosphate slurry: Microscopic analysis, cellular response, and animal experiment. Journal of
451   Biomedical Materials Research Part B Applied Biomaterials 106: 2716-2724
452   DOI:10.1002/jbm.b.34089.

453   7. Minko D, Belyavin K, Sheleg V. 2017. Biomechanical properties of composite

454   compact-porous titanium produced by electric discharge dintering. IOP Conference Series

455   Materials Science and Engineering DOI:10.1088/1757-899X/218/1/012008.

456   8. Lai M, Cai K, Hu Y, Yang X, Liu Q. 2012. Regulation of the behaviors of mesenchymal

457   stem cells by surface nanostructured titanium. Colloids Surf. B 97:211-220
458   DOI:10.1016/j.colsurfb.2012.04.029.

459   9. T.H. Fang, W.L. Li, N.R. Tao, K. Lu. 2011. Revealing extraordinary intrinsic tensile

460   plasticity in gradient nano-grained copper. Science 331:1587-1590
461   DOI:10.1126/science.1200177.

462   10. Z.B. Wang, K. Lu. 2017. Diffusion and surface alloying of gradient nanostructured

463   metals. Beilstein J. Nanotechnol 8:547-560 DOI: 10.3762/bjnano.8.59.

464   11. W.P. Tong, N.R. Tao, Z.B. Wang, J. Lu, K. Lu. 2003. Nitriding iron at lower

465   temperatures. Science 299:686-688 DOI: 10.1126/science.1080216.

466   12. Z.B. Wang, N.R. Tao, S. Li, W. Wang, G. Liu, J. Lu, K. Lu. 2003. Effect of surface

467   nanocrystallization on friction and wear properties in low carbon steel. Mater. Sci. Eng. A

468   352:144-149 DOI:10.1016/S0921-5093(02)00870-5.

469   13. Y.B. Lei, Z.B. Wang, J.L. Xu, K. Lu. 2019. Simultaneous enhancement of stress-

470   and strain-controlled fatigue properties in 316L stainless steel with gradient nanostructure.

471   Acta Mater 168:133-142.

472   14. Lu K, Lu J. 2004. Nanostructured surface layer on metallic materials induced by

473   surface mechanical attrition treatment. Mater. Sci. Eng. A 375-377:38-45

474   DOI:10.1016/j.msea.2003.10.261.

475   15. Son JW, Kim BC, Yoon JH, Lee J, Lim HJ. 2018. Mandibular Regeneration With

476   Autologous Human Bone Marrow Derived Mesenchymal Stem Cells to Treat Unicystic

477   Ameloblastoma. Journal of Craniofacial Surgery 30:1 DOI:10.1097/SCS.0000000000004917

478   16. Miranda H C , Herai R H , Carolina Hassibe Thomé, Gomes GG, Panepucci RA,

479   Orellana MD, Covas DT, Muotri AR, Greene LJ, Faça VM. 2012. A quantitative

480   proteomic and transcriptomic comparison of human mesenchymal stem cells from bone

481   marrow and umbilical cord vein. PROTEOMICS 12:2607-2617

482   DOI:10.1002/pmic.201200111.

483   17. Zhao R, Li F Q, Tian L L, Shang DS, Guo Y, Zhang JR, Liu M. 2019. Comprehensive

484   analysis of the whole coding and non-coding RNA transcriptome expression profiles and

485   construction of the circRNA–lncRNA co-regulated ceRNA network in laryngeal squamous

486   cell carcinoma. Functional & Integrative Genomics 19:109-121 DOI:10.1007/s10142-018-

487   0631-y.

488   18. Ji HN, Kim KM, Mcclusky WG, Abdelmohsen K, Gorospe M. 2018. Cytoplasmic

489   functions of long noncoding RNAs. Wiley Interdisciplinary Reviews Rna 9:e1471

490   DOI:10.1002/wrna.1471.

491   19. Liu J, Liu T, Wang X, He A. 2017. Circles reshaping the RNA world: from waste

492   to treasure. Molecular Cancer 16:58 DOI:10.1186/s12943-017-0630-y.

493   20. Zhao Z, Wang K, Wu F, Wang W, Zhang K, Hu H, Liu Y, Jiang T. 2018. circRNA disease:

494   a manually curated database of experimentally supported circRNA-disease associations.

495   Cell Death & Disease, 9:475.

496   21. Zhang M, Xin Y. 2018. Circular RNAs: a new frontier for cancer diagnosis and therapy.

497   Journal of Hematology & Oncology 11:21.

498   22. Kulcheski F R, Christoff A P, Margis R. 2016. Circular RNAs are miRNA sponges and

499   can be used as a new class of biomarker. Journal of Biotechnology

500   238:S0168165616315292 DOI:10.1016/j.jbiotec.2016.09.011.

501   23. Cortéslópez M, Gruner M R, Cooper D A, Gruner HN, Voda AI, Linden AMvd, Miura P.

502   2018. Global accumulation of circRNAs during aging in Caenorhabditis elegans. Bmc

503   Genomics 19:8 DOI:10.1186/s12864-017-4386-y.

504   24. Li S, Han L. 2019. Circular RNAs as promising biomarkers in cancer: detection, function,

505   and beyond. Genome Medicine 11:15 DOI:10.1186/s13073-019-0629-7.

506   25. Mengjun Z, Lingfei J, Yunfei Z. 2018. circRNA Expression Profiles in Human Bone

507   Marrow Stem Cells Undergoing Osteoblast Differentiation. Stem Cell Reviews and Reports

508   15:126-138 DOI:10.1007/s12015-018-9841-x.

509   26. Zheng Y, Li X, Huang Y, Jia L, Li W. 2017. The Circular RNA Landscape of Periodontal

510   Ligament Stem Cells During Osteogenesis. Journal of Periodontology 88:906-914

511   DOI:10.1902/jop.2017.170078.

512   27.   Nana L, Ning W. 2018. The effect of duplex Surface mechanical attrition and nitriding

513   treatment on corrosion resistance of stainless steel 316L. Scientific Reports 8:8454

514   DOI:10.1038/s41598-018-26844-0.

515   28. Du H, An Y, Zhang X, Wei Y, Hou L, Liu H, Zhang J, Wang N, Umar A, Guo Z. 2019.

516   Hydroxyapatite (HA) Modified Nanocoating Enhancement on AZ31 Mg Alloy by

517   Combined Surface Mechanical Attrition Treatment and Electrochemical Deposition

518   Approach. Journal of Nanoscience and Nanotechnology 19:810-818

519   DOI:10.1166/jnn.2019.15746.

520   29. Nowak W J, Serafin D, Wierzba B. 2019. Effect of surface mechanical treatment on the

521   oxidation behavior of FeAl-model alloy. Journal of Materials Science, 54:9185-9196.

522   30. Benafia S, Retraint D, Brou S Y. 2018. Influence of Surface Mechanical Attrition

523   Treatment on the oxidation behaviour of 316L stainless steel. Corrosion Science 136:188-

524   200.

525   31. Yao Q, Sun J, Zhang G, Tong W, Zhang H. 2017. Thermal Stability of Nanocrystalline

526   BCC-Ti Formed by Phase Transformation During Surface Mechanical Attrition Treatment.

527   Nano 12:1750113 DOI:10.1142/S1793292017501132.

528   32. Saito A, Nagaishi K, Iba K, Yuka Mizue, Chikenji T, Otani M, Nakano M, Oyama K,

529   Yamashita T, Fujimiya M. 2018. Umbilical cord extracts improve osteoporotic

530   abnormalities of bone marrow-derived mesenchymal stem cells and promote their

531   therapeutic effects on ovariectomised rats. Scientific Reports 8:1161 DOI:

532   10.1038/s41598-018-19516-6.

533   33. Mohammadali F, Abroun S, Atashi A. 2018. Mild hypoxia and human bone marrow

534   mesenchymal stem cells synergistically enhance expansion and homing capacity of human

535   cord blood CD34+ stem cells. Iranian Journal of Basic Medical Sciences 21:709-716 DOI:

536   10.22038/ijbms.2018.26820.6561.

537   34. Amini A, Pouriran R, Abdollahifar M A, Abbaszadeh HA, Ghoreishi SK, Chien S, Bayat

538   M. 2018. Stereological and molecular s tudies on the combined effects of

539   photobiomodulation and human bone marrow mesenchymal stem cell conditioned medium

540   on wound healing in diabetic rats. Journal of Photochemistry and Photobiology B: Biology

541   182:42-51.

542   35. Mohammadali F, Abroun S, Atashi A. 2018. Mild hypoxia and human bone marrow
543   mesenchymal stem cells synergistically enhance expansion and homing capacity of human
544   cord blood CD34+ stem cells.Iranian Journal of Basic Medical Sciences 21:709-716 DOI:

545   10.22038/ijbms.2018.26820.6561.

546   36. Liu C, Feng X, Wang B, Wang X, Wang C, Yu M, Cao G, Wang H. 2018. Bone marrow
547   mesenchymal stem cells promote head and neck cancer progression through
548   Periostin-mediated phosphoinositide 3-kinase/Akt/mammalian target of rapamycin. Cancer
549   Science 109:688-698 DOI:10.1111/cas.13479.

550   37. Gabr MM, Zakaria MM, Refaie AF, Rahman EAA, Rahman EAA, Reda AM. Ali SS,

551   Khater SM, Ashamallah SA, Ismail AM, Ismail HEDA, Badri NE, Ghoneim MA. 2017. From

552   Human Mesenchymal Stem Cells to Insulin-Producing Cells: Comparison between Bone

553   Marrow- and Adipose Tissue-Derived Cells. Biomed Research International 2017:1-9

554   DOI:10.1155/2017/3854232.

555   38. Lee H J, Kim S N, Jeon M S, Yi TG, Song SU. 2017. ICOSL expression in human bone
556   marrow-derived mesenchymal stem cells promotes induction of regulatory T cells.
557   Scientific Reports 7:44486 DOI:10.1038/srep44486.

558   39. Zhu W Q, Ming P P, Jing Q,Shao SY, Yu YJ, Chen JX, Yang J, Xu LN, Zhang SM, Tang
559   CB. 2018. Effect of titanium ions on the Hippo/YAP signaling pathway in regulating
560   biological behaviors of MC3T3-E1 osteoblasts. Journal of Applied Toxicology 38:824-833
561   DOI:10.1002/jat.3590.

562   40. Urbanek K, Lesiak M, Krakowian D, Komarska HK, Likus W, Czekaj P,Kusz
563   D, Sieroń AL. 2017. Notch signaling pathway and gene expression profiles during early in
564   vitro differentiation of liver-derived mesenchymal stromal cells to osteoblasts. Laboratory
565   Investigation 97:1225-1234 DOI:10.1038/labinvest.2017.60.

566   41. Jin L, Cao Y, Yu G, Wang J, Lin X, Ge L, Du J, Wang L, Diao S, Lian X, Wang
567   S, Dong R, Shan Z. 2017. SFRP2 enhances the osteogenic differentiation of apical papilla

568   stem cells by antagonizing the canonical WNT pathway. Cellular & Molecular Biology
569   Letters 22:14 DOI:10.1186/s11658-017-0044-2.

570   42. Yang S, Yu Y, Shuang Z, Wang J, Xiao Y, Liu C. 2018. The immunomodulatory role of
571   sulfated chitosan in BMP-2-mediated bone regeneration. Biomaterials Science 6:2496-2507
572   DOI:10.1039/C8BM00701B.

573   43. Hui L, Zhang S, Nie B, Long T, Qu X, Yue B. 2018. The antimicrobial peptide KR-12
574   promotes the osteogenic differentiation of human bone marrow stem cells by stimulating
575   BMP/SMAD signaling. Rsc Advances 8:15547-15557 DOI:10.1039/c8ra00750k.

576   44. Lou R, Dong S, Shi C, Shi C, Xu X, Ma R, Wu J, Feng J. 2019. Liver X receptor agonist
577   T0901317 inhibits the migration and invasion of non-small-cell lung cancer cells in vivo
578   and in vitro. Anticancer Drugs 30:495-500 DOI:10.1097/CAD.0000000000000758.

579   45. Jiang L, Wang Y, Liu G, Liu H, Zhu F, Ji H, Li B. 2018. C-Phycocyanin exerts anti-cancer
580   effects via the MAPK signaling pathway in MDA-MB-231 cells. Cancer Cell International
581   18:12 DOI:10.1186/s12935-018-0511-5.

582   46. Li Z H, Li L, Kang L P, Wang Y. 2018. MicroRNA-92a promotes tumor growth and
583   suppresses immune function through activation of MAPK/ERK signaling pathway by
584   inhibiting PTEN in mice bearing U14 cervical cancer. Cancer Medicine 7: 3118–3131
585   DOI:10.1002/cam4.1329.

586   47. Wang X, Wang X, Liu Y, Dong Y, Wang Y, Kassab MA, Fan W, Yu X, Wu C. 2019.
587   LGR5 regulates gastric adenocarcinoma cell proliferation and invasion via activating Wnt
588   signaling pathway. Oncogenesis 8:57 DOI:10.1038/s41389-018-0071-5.

589   48. Shuai Y, Yang R, Mu R, Yu Y, Rong L, Jin L. 2019. MiR-199a-3p mediates the
590   adipogenic differentiation of bone marrow-derived mesenchymal stem cells by regulating
591   KDM6A/WNT signaling. Life Sciences 220:84-91 DOI:10.1016/j.lfs.2019.01.051.

592   49. Hang K , Ye C, Xu J, Chen E, Wang C, Zhang W, Ni L, Kuang Z, Ying K, Xue D, Pan Z.
593   2019. Apelin enhances the osteogenic differentiation of human bone marrow mesenchymal
594   stem cells partly through Wnt/β-catenin signaling pathway. Stem Cell Research & Therapy

595   10:189 DOI:10.1186/s13287-019-1286-x.

596   50. Jun-Li Liu, Kaddour N, Chowdhury S, Li Q, Gao ZH. 2017. Role of CCN5 (WNT1

597   inducible signaling pathway protein 2) in pancreatic islets. Journal of Diabetes 9:462-474

598   DOI:10.1111/1753-0407.12507.

599   51. Nandagopal N, Santat LA, LeBon L, Sprinzak D, Bronner ME, Elowitz MB. 2018.

600   Dynamic Ligand Discrimination in the Notch Signaling Pathway. Cell

601   172:S0092867418300023 DOI:10.1016/j.cell.2018.01.002.

602   52. Sun Z, Cheng Z, Feng L, Zhang W, Chen J, Pan Y, Ma L, Liu Q, Du Y, Yang J, Wang Q.

603   2018. Inhibition of breast cancer cell survival by Xanthohumol via modulation of the Notch

604   signaling pathway in vivo and in vitro. Oncology Letters 15:908-916

605   DOI:10.3892/ol.2017.7434.

606   53. Carra S, Sangiorgio L, Pelucchi P, Cermenati S, Mezzelani A, Martino V, Palizban

607   M, Albertini A, Götte M, KehlerJ, Deflorian G, Beltrame M, Giordano A, Reinbold R, Cote

608   lli F, Bellipanni G, Zucchi I. 2017. Zebrafish Tmem230a cooperates with the Delta/Notch

609   signaling pathway to modulate endothelial cell number in angiogenic vessels. Journal of

610   Cellular Physiology 233:1455-1467 DOI:10.1002/jcp.26032.

611   54. Gu X, Li M, Jin Y, Liu D, Wei F. 2017. Identification and integrated analysis of

612   differentially expressed lncRNAs and circRNAs reveal the potential ceRNA networks

613   during PDLSC osteogenic differentiation. BMC Genetics 18:100 DOI:10.1186/s12863-017-

614   0569-4.

615   55. Xiaobei L, Yunfei Z, Yan Z, Huang Y, Zhang Y, Jia L, Li W. 2018. Circular RNA

616   CDR1as regulates osteoblastic differentiation of periodontal ligament stem cells via the

617   miR-7/GDF5/SMAD and p38 MAPK signaling pathway. Stem Cell Research & Therapy

618   9:232 DOI:10.1186/s13287-018-0976-0.

619   56. Samuel S, Ahmad RE, Ramasamy TS, Karunanithi P, Naveen SV, Murali MR, Abbas

620   AA, Kamarul T. 2016. Platelet-rich concentrate in serum free medium enhances osteogenic

621   differentiation of bone marrow-derived human mesenchymal stromal cells. PeerJ 4:e2347

622   DOI:10.7717/peerj.2347.

623   57. Li R, Sun J, Yang F, Sun Y, Wu X, Zhou Q, Yu Y, Bi W. 2019. Effect of GARP on

624   osteogenic differentiation of bone marrow mesenchymal stem cells via the regulation of

625   TGFβ1 in vitro. PeerJ 7:e6993 DOI:10.7717/peerj.6993.

626   58. Kureel J, John A A, Prakash R, Singh D. 2017. MiR 376c inhibits osteoblastogenesis by

627   targeting Wnt3 and ARF-GEF-1 facilitated augmentation of beta-catenin transactivation.

628   Journal of Cellular Biochemistry 119: 3293-3303 DOI:10.1002/jcb.26490.

629   59. Qin X, Jiang Q, Matsuo Y, Kawane T, Komori H, Moriishi T, Taniuchi I, Ito K, Kawai

630   Y, Rokutanda S, Izumi S, Komori T. 2015. Cbfb regulates bone development by

631   stabilizing runx family proteins. Journal of Bone and Mineral Research 30: 706-714

632   DOI:10.1002/jbmr.2379.

633   60. Lindsey R C , Rundle C H , Mohan S. 2018. Role of IGF-I and Efn-Eph signaling

634   in skeletal metabolism. Journal of Molecular Endocrinology 61:JME-17-0284 DOI:

635   10.1530/JME-17-0284.

636   61. Mobini S, Leppik L, Thottakkattumana Parameswaran V, Barker JH. 2017. In

637   vitro effect of direct current electrical stimulation on rat mesenchymal stem

638   cells. PeerJ 5:e2821 DOI:10.7717/peerj.2821.

639   62. Li R, Sun J, Yang F, Sun Y, Wu X, Zhou Q, Yu Y, Bi W. 2019. Effect of GARP on

640   osteogenic differentiation of bone marrow mesenchymal stem cells via the regulation of

641   TGFβ1 in vitro. PeerJ 7:e6993 DOI:10.7717/peerj.6993

642   63. Mao X Y , Bian Q , Shen Z Y. 2012. Analysis of the osteogenetic effects exerted on

643   mesenchymal stem cell strain C3H10T1/2 by icariin via MAPK signaling pathway in vitro.

644   Journal of Chinese Integrative Medicine 10:1272-1278 DOI:10.4236/ojemd.2015.52002.

645

646

647

Primer and internal reference gene sequence table.

1   Table 1:

2   Primer and internal reference gene sequence table.

Name of circRNA/ internal reference	Primer sequence(5'-3')	Product length(bp)
hsa-circ-0032599	CTGGAACCTGCGTGAACCT TGATCCGCTGGGCCAAAG	226
hsa-circ-0032600	CTGGAACCTGCGTGAACCT TCTTGGCAGTGAGTGAGGTT	221
hsa-circ-0032601	CTGGAACCTGCGTGAACCT TGGTGGATCTGCACTGAGG	229
GAPDH	GGACCTGACCTGCCGTCTAG TAGCCCAGGATGCCCTTGAG	99

Predicted miRNAs and their gene symbols, signaling pathways.

Table 2 Predicted miRNAs and their gene symbols, signaling pathways.

miRNA	gene symbol	signaling pathway
hsa-miR-18b-5p	ABCA3	
hsa-let-7b-5p	HERC1	
hsa-miR-1224-5p	MCF2L2、PLPPR4、SPEG	
hsa-miR-129-5p	FAT3、LTBP2、MYH9、SMARCA2、TBC1D2B、VPS13C、DYNC1H1	
	DGKD	Phospholipase D 、Gastrin-CREB via PKC and MAPK
hsa-miR-145-5p	BRPF3、TANGO6	
	COL4A2	AGE-RAGE、ERK 、FAK1 、GnRH 、ILK
hsa-miR-24-3p	ADAMTS13、DIP2C、SYNM	
hsa-miR-5195-3p	ARHGAP32、CCDC88C、FLNA、LTBP2、MDN1、RAB31、TBCD、TRIOBP	
	GNB5	Corticotropin-releasing hormone 、G Protein 、Apelin 、Chemokine 、Chemotaxis CXCR4
hsa-miR-6088	CARD8	NOD-like receptor
	KMT2A	
hsa-miR-18b-5p	ABCA3	
hsa-let-7b-5p	HERC1	
hsa-miR-1224-5p	MCF2L2、PLPPR4、SPEG	
hsa-miR-129-5p	FAT3、LTBP2、MYH9、SMARCA2、TBC1D2B、VPS13C、DYNC1H1	

1		DGKD	Phospholipase D 、 Gastrin-CREB via PKC and MAPK
2	hsa-miR-145-5p	BRPF3、TANGO6	
3		COL4A2	AGE-RAGE、ERK 、FAK1 、GnRH 、ILK
	hsa-miR-24-3p	ADAMTS13、DIP2C、SYNM	
	hsa-miR-5195-3p	ARHGAP32、CCDC88C、FLNA、LTBP2、MDN1、RAB31、TBCD、TRIOBP	
		GNB5	Corticotropin-releasing hormone 、G Protein 、Apelin 、Chemokine 、Chemotaxis CXCR4
	hsa-miR-6088	CARD8	NOD-like receptor
		KMT2A	

Predicted circRNAs and their chrs, gene symbols, miRNAs, signaling pathways.

1   Table 3 Predicted circRNAs and their chrs, gene symbols, miRNAs, signaling pathways.

chr	hsa_circRNA	gene symbol	miRMA	signaling pathway
chr10	hsa_circ_0076184	BRPF3	hsa-miR-129-5p	
	hsa_circ_0002749	CARD8	hsa-miR-129-5p	NOD-like receptor
chr13	hsa_circ_0051734	CARD8	hsa-miR-129-5p	NOD-like receptor
chr	hsa_circRNA	gene symbol	miRMA	signaling pathway
chr14	hsa_circ_005173 hsa_circ_0051736	CARD8	hsa-miR-129-5p	NOD-like receptor
	hsa_circ_0030878	COL4A2	hsa-miR-129-5p	AGE-RAGE、ERK、FAK1 、GnRH、ILK
	hsa_circ_0058776	DGKD	hsa-miR-129-5p	Phospholipase D、Gastrin-CREB via PKC and MAPK
	hsa_circ_0017364 hsa_circ_0017365	DIP2C	hsa-miR-129-5p	
chr15	hsa_circ_0091990 hsa_circ_0091991 hsa_circ_0091992 hsa_circ_0091997 hsa_circ_0091998 hsa_circ_0091999 hsa_circ_0092000 hsa_circ_0092001 hsa_circ_0092008 hsa_circ_0092009 hsa_circ_0092010	FLNA	hsa-miR-145-5p	
		FLNA	hsa-miR-145-5p	
	hsa_circ_0035311 hsa_circ_0035312 hsa_circ_0035313	GNB5	hsa-miR-24-3p	Corticotropin-releasing hormone、G Protein、Apelin、Chemokine、Chemotaxis CXCR4
	hsa_circ_0032566 hsa_circ_0032576 hsa_circ_0032579 hsa_circ_0032584 hsa_circ_0032585	LTBP2	hsa-miR-24-3p	

chr	hsa_circRNA	gene symbol	miRMA	signaling pathway
chr17	hsa_circ_0032594 hsa_circ_0032599 hsa_circ_0032600 hsa_circ_0032601 hsa_circ_0032602 hsa_circ_0032604 hsa_circ_0032605 hsa_circ_0032607 hsa_circ_0032608	LTBP2	hsa-miR-24-3p	

chr	hsa_circRNA	gene symbol	miRMA	signaling pathway
chr17	hsa_circ_0077356 hsa_circ_0077360 hsa_circ_0077371	MDN1	hsa-miR-5195-3p	
chr18	hsa_circ_0077375	MDN1	hsa-miR-5195-3p	
	hsa_circ_0063112	MYH9	hsa-miR-5195-3p	
chr19	hsa_circ_0063114 hsa_circ_0063115 hsa_circ_0063117	MYH9	hsa-miR-5195-3p	
	hsa_circ_0046890	RAB31		
chr2	hsa_circ_0046891	RAB31		
chr22	hsa_circ_0037043	SYNM	hsa-miR-5195-3p	
	hsa_circ_0036435 hsa_circ_0036436 hsa_circ_0036437	TBC1D2B	hsa-miR-6088	
chr6	hsa_circ_0036438 hsa_circ_0036439 hsa_circ_0036440 hsa_circ_0036441	TBC1D2B	hsa-miR-6088	
	hsa_circ_0046529	TBCD	hsa-miR-6088	
chrx	hsa_circ_0046568 hsa_circ_0046569 hsa_circ_0046577 hsa_circ_0046588 hsa_circ_0046589 hsa_circ_0046590 hsa_circ_0046591	TBCD	hsa-miR-6088	

hsa_circ_0046594
hsa_circ_0046595
hsa_circ_0046596
hsa_circ_0035596   VPS13C   hsa-miR-6088

Figure 1

The TEM observation of the gradient nano-metal pure titanium.
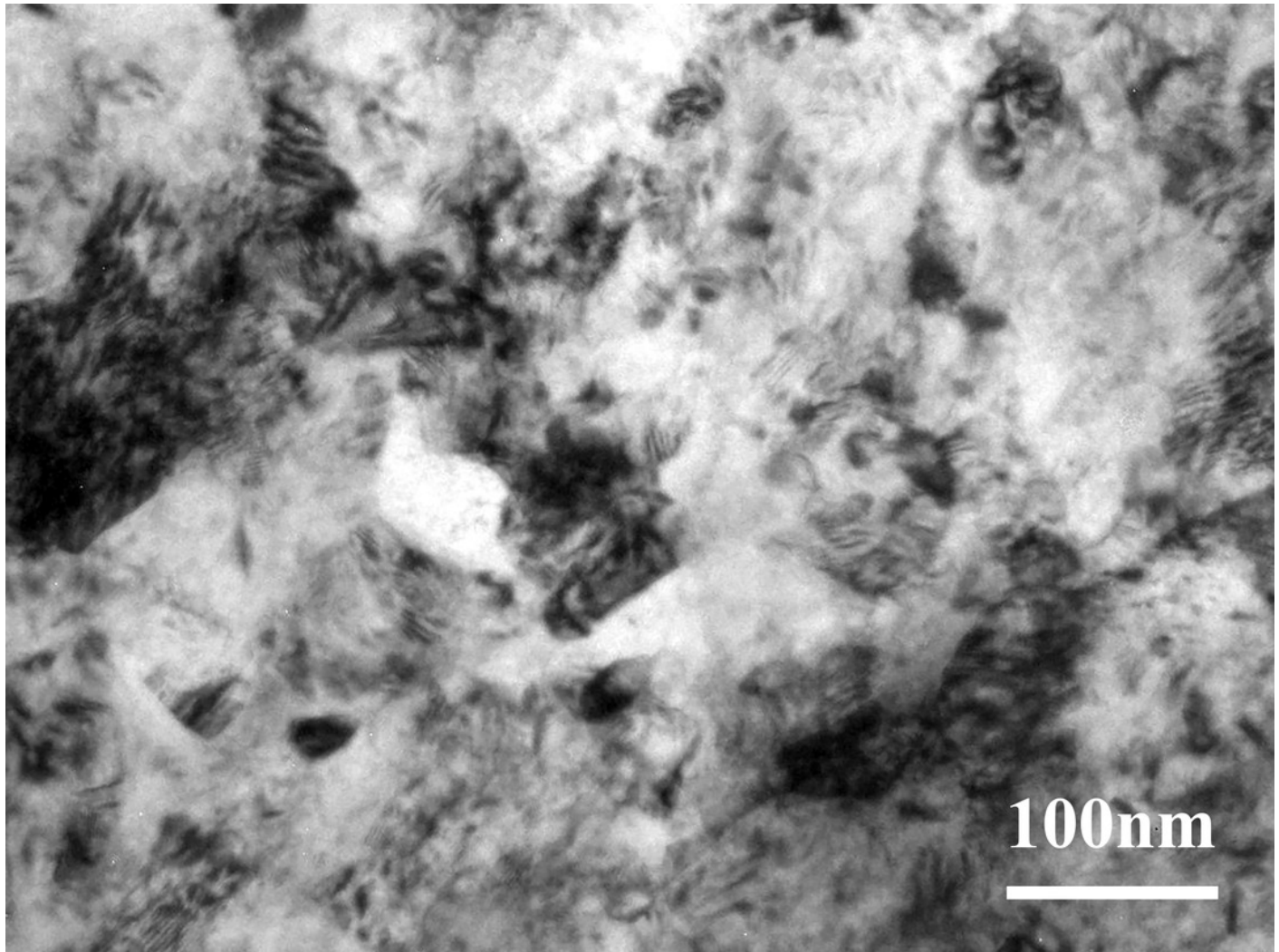
Figure 2

Culture and proliferation curve of the hBMSCs.

(A) HBMSCs cultured for 1 day (x100). (B) HBMSCs cultured for 3 days (x100). (C) CCK8 detection at 1, 3, 5, and 7 days of hBMSCs culture. *: The SMAT group compared with the annealed group. (mean ± SD, n = 3, * indicates $p < 0.05$).
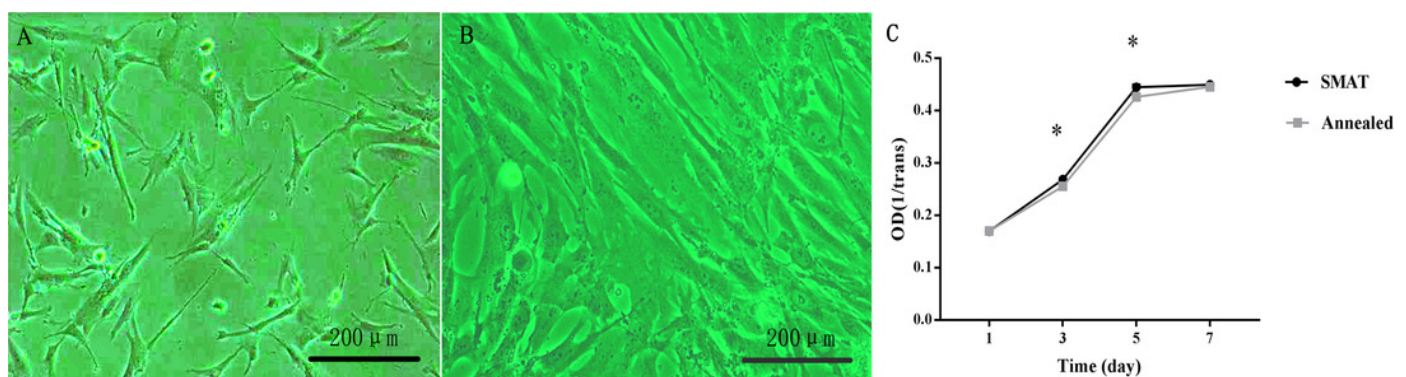
Figure 3

Detection of ALP activity and alizarin red staining of hBMSCs.

(A) Alizarin red staining after osteogenic induction of hBMSCs for 7 days, (B) 14 days and (C) 21 days. (D) Detection of ALP activity at 3, 5, 7 and 14 days after osteogenic induction of hBMSCs. *: The SMAT group compared with the annealed group. (mean ± SD, n = 3, * indicates $p < 0.05$). (E) The area of alizarin red staining at 7, 14, 21 days after osteogenic induction of hBMSCs. *: The SMAT group compared with the annealed group. (mean ± SD, n = 3, * indicates $p < 0.05$).
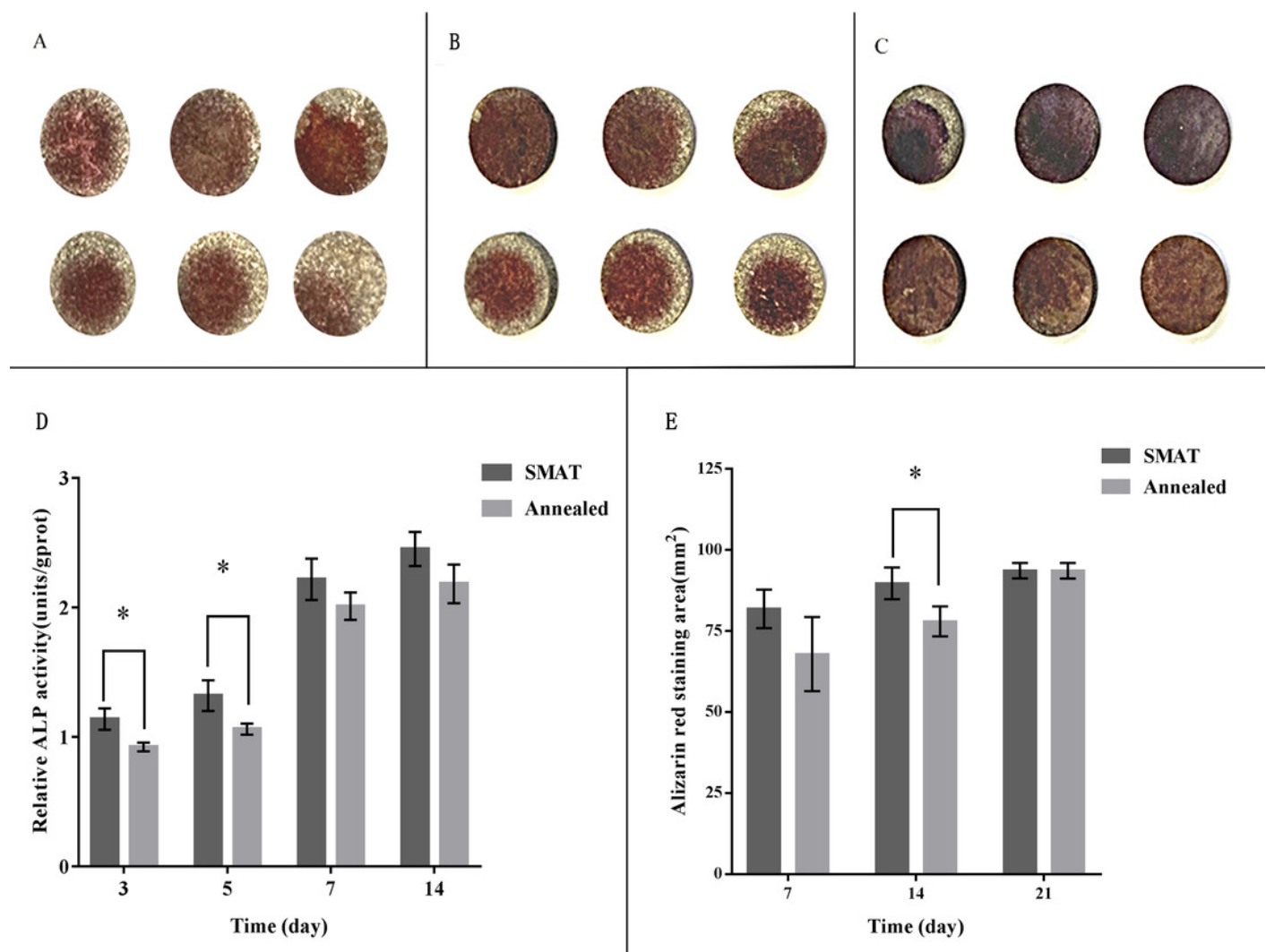
Figure 4

Biological information prediction.

(A) Numbers of circRNAs corresponding to different chrs. (B) Numbers of circRNAs on different signaling pathways. (C-L) Genes in the signaling pathways. (M) Network analysis of osteogenesis-related miRNAs and their interacting circRNAs and target genes.
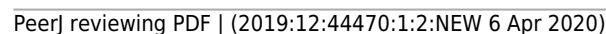
Figure 5

QRT-PCR results of the three differentially expressed circRNAs.

*: The SMAT group compared with the annealed group, FC >2.0. (mean ± SD, n = 3, * indicates $p< 0.05$).